VOL. 13, NO. 20, OCTOBER 2018 ISSN 1819-6608
ARPN Journal of Engineering and Applied Sciences

www.arpnjournals.com

PHYSICAL AND ELECTRICAL ANALYSES OF SOLID POLYMER ELECTROLYTES

M. F. Hassan[1,2] and H. K. Ting[3]
[1]Advanced Nano Materials (ANoMa) Research Group, Universiti Malaysia Terengganu, Kuala Nerus, Terengganu, Malaysia
[2]School of Fundamental Science, Universiti Malaysia Terengganu, Kuala Nerus, Terengganu, Malaysia
[3]School of Ocean Engineering, Universiti Malaysia Terengganu, Kuala Nerus, Terengganu, Malaysia
E-Mail: mfhassan@umt.edu.my

ABSTRACT

In this work, we prepared a solid polymer electrolyte based on starch and sodium hydroxide via a simple casting method. The hybrid starch–sodium hydroxide film formed the belts morphology. Such belt structure is believed to be able to improve ionic mobility and electrochemical reaction effectively. The highest ionic conductivity was achieved at 3.93 x 10^{-3} S/cm for 25 wt% of sodium hydroxide. A comparative investigation on sodium hydroxide as an ionic dopant in starch proved that the sodium hydroxide addition is an effective way to increase ionic conductivity and electrochemical activity.

Keywords: solution casting technique, solid polymer electrolyte, starch, sodium hydroxide, ionic conductivity, physical analyses, electrical conductivity.

INTRODUCTION

Solid polymer electrolyte (SPE) systems are promising candidates for all–solid state storage devices. These SPEs are known to have a lot of advantages such as no possibility of leaks, ability to strengthen devices due to its all–solid state construction, shape flexibility, low device weight as all–solid state devices do not need heavy metal casing, prevention of dendrite development, better overheat, wider operating temperature (–40°C to 150°C compared to liquid electrolyte at −15°C to 60°C), and improved cell safety. The materials used in solid polymer electrolyte systems are inexpensive, environmental–friendly and exist in abundance in nature. However, its conductivity at room temperature is not high enough for application in batteries. A highly resistive layers formation at the anode–electrolyte interface provides another disadvantage.

Many researchers have been implemented SPEs as one of the components in their all–solid state devices [1–8]. Singh *et al.* had tested the performance of a solid–state battery with a $Zn/ZnSO_4.7H_2O/I_2$configuration [1]. The cell was given an open-circuit voltage of 1.1V, a short–circuit current of more than 10mA and an energy density of 13.8Whkg^{-1} at a constant–current drain of 100μA. The cells based on the Zn/PVA–KOH/MnO_2 configuration conducted by [4] claimed that its open circuit potential had reached above 1.5 V. A plateau of cell voltage was shown in the discharge curves ranging from 1.3 to 1.1 V. The cell discharge capacity of ca. 210 mAh g^{-1} was obtained per gram of MnO_2 mass for 1mA constant discharge current and exhibited good discharge characteristics and stability of the electrolyte. Hiralal *et al.* studied the mechanical stressed conditions of the all–solid state and flexible zinc carbon batteries [2]. By using a solid polymer electrolyte in the battery fabrication, the results showed that improvements in terms of battery shelf life and solid–state mechanical flexibility can be achieved. Similar results were also obtained by Fu *et al.* on a flexible solid–state electrolyte used in a rechargeable zinc–air battery system [3]. The system which used a nano–porous alkaline-exchange electrolyte membrane from natural cellulose nano–fiber exhibited high ionic–conductivity and water retention as well as high bending flexibility. These advantages render the membrane as a promising solid–state electrolyte for rechargeable zinc–air batteries in lightweight and flexible electronic applications. All of these novel works provide proof that the SPEs have potential in solid–state battery applications. Hence, SPEs based on starch complexed with sodium salts would be the next new system to be explored.

Starch is a carbohydrate extracted from agricultural raw materials which extensively exist in factually thousands of daily food and non–food applications. Since it is renewable and biodegradable, it is also an impeccable raw material to be used as a substitute for fossil–fuel components in various chemical applications such as plastics, detergents, glues etc. Its potential as one of the components of interest in electrochemical storage devices provides extra advantages for advanced exploration [9-13].

NaOH is known as a caustic soda. It is an inorganic compound with the formula NaOH. It is a white solid ionic compound consisting of sodium cations Na^+ and hydroxide anions OH^-. It is used in many industries, including electrochemical applications [14-17]. Earlier studies have revealed that NaOH could improve some electrochemical properties of the energy storage systems in terms of its energy density and voltaic efficiency.

To the best of our knowledge, studies on a starch–NaOH solid polymer electrolyte hybrid are very rare. Therefore, this study is focused on the evaluation of the microstructure, crystallization behavior and electrical properties of the starch–NaOH films. Moreover, this study is based on our recent reports on poly (sodium 4-styrenesulfonate)–$LiClO_4$ and poly (sodium 4-styrenesulfonate)–NH_4NO_3 films [18, 19]. The material

produced involves degradable polymers, and thus is more biodegradable.

MATERIALS AND EXPERIMENTAL METHODS

Sample preparation

Starch (derived from corn) and NaOH were purchased from Aldrich and Sigma–Aldrich, respectively. Concisely, two different solvents (25 ml distilled water and 0.6 ml glycerin) were mixed together under a temperature of 70 ^{o}C. Starch powder (1g) was added to the prepared solution under vigorous mechanical stirring. Next, NaOH concentrations (varied from 0 to 30 (in weight percentage, wt.%)) were added to the solution as scheduled in Table-1. The mixtures were stirred continuously until homogenous solutions were achieved. The solutions were poured into different plastic Petri dishes and left for thin film formation. The films were then kept in desiccators for a certain period to ease water content. All the experimental steps were conducted at room temperature. To note here, the weight in gram of NaOH was calculated using Equation 1 as follows:

$$wt.\% = \frac{x}{x+y} \times 100 \quad (1)$$

where x is the amount of dopant in gram (g), y is the amount of starch, and weight percentage is the varying values of dopant in percentage form. All the experimental steps were carried out at room temperature and described in Figure-1.

Table-1. The compositions of starch and NaOH powders.

Sample	Solvent (ml)		Starch (g)	Ionic salt (wt.%)	
	Water	Glycerin			Ionic salt (g)
Pure	25	0.6	1	0	0
A	25	0.6	1	5	0.053
B	25	0.6	1	10	0.111
C	25	0.6	1	15	0.176
D	25	0.6	1	20	0.250
E	25	0.6	1	25	0.333
F	25	0.6	1	30	0.429

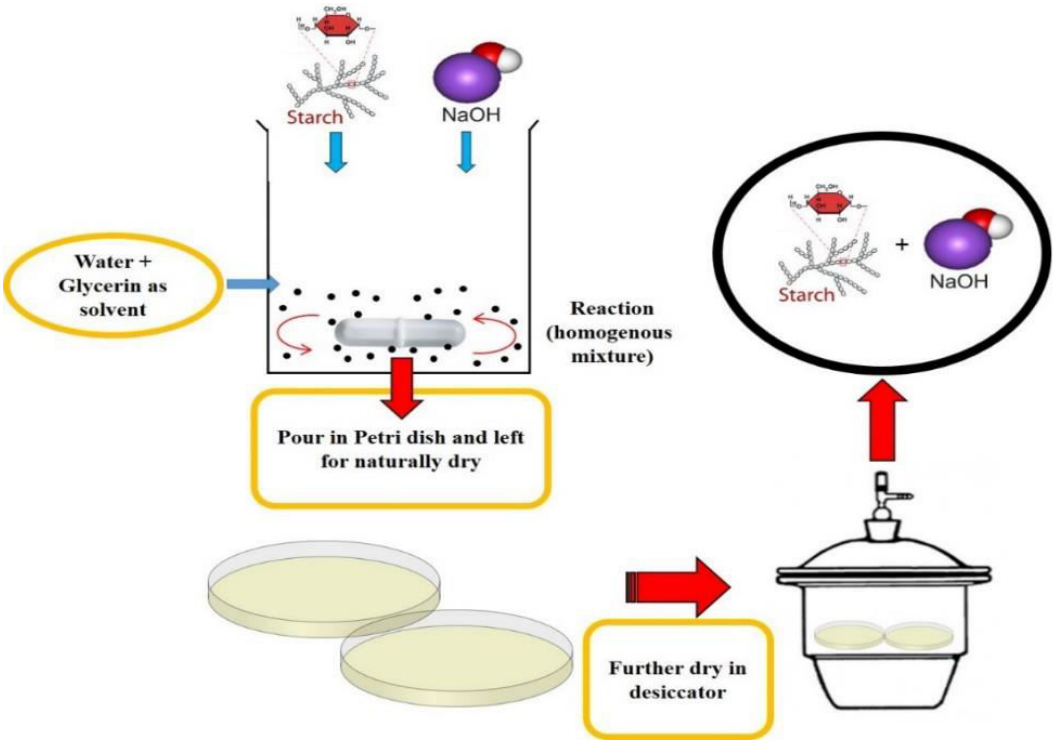

Figure-1. A schematic diagram to prepare starch-NaOH complex films.

Characterizations

An X–ray diffraction (XRD) analysis was performed using a MiniFlex II diffractometer equipped with an X' celerator using CuKα operated at 40 kV and 30 mA to record diffractogram in the range of 2θ = 10° to 80°.

Fourier transform infrared (FTIR) spectra of the pure starch and hybrid starch–NaOH were recorded using a Thermo Nicolet Avatar 380 FT–IR spectrometer at a resolution of 4 cm^{-1} in the wave number range of 675 to 4000 cm^{-1}.

Micrographs of film surfaces were investigated using scanning electron microscopy (SEM) at an acceleration voltage of 20kV using JEOL JSM–6360LA under magnifications of x300 to x10000, accordingly. Prior to the SEM observations, the samples were coated with a fine gold layer.

Impedance analysis was measured using a HIOKI 3532–02 LCR Hi–Tester interfaced with a computer over a frequency range of 50Hz to 1MHz. The prepared samples were cut to 2 cm diameter size and positioned between two stainless steel electrodes on a sample holder which were connected via lead to a computer. The imaginary impedance (Z_i) versus the real impedance (Z_r) was plotted using the same scale for both vertical and horizontal axes in order to obtain the bulk resistance, R_b. A micrometer–screw gauge was used to measure the sample thickness, and the sample conductivity was calculated using the Equation (2) as follows:

$$\sigma = \frac{t}{R_b A} \quad (2)$$

where t is the thickness of the thin film (in cm), and A is the area of the contact and R_b is bulk resistance.

RESULTS AND DISCUSSIONS

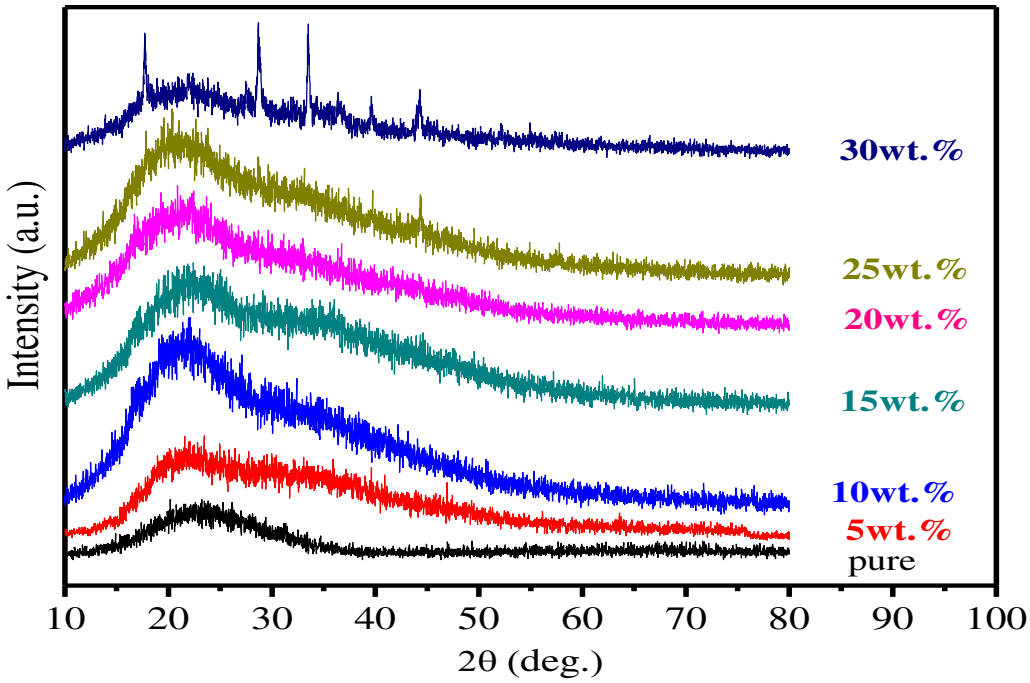

Figure-2. XRD patterns for starch and hybrid starch–NaOH films.

The XRD patterns of the starch and hybrid starch–NaOH films are shown in Figure-2. The pure starch diffraction pattern can be acknowledged with a broad peak of 2θ (15° to 27°). As discussed by some researchers, this peak is a combination of several peaks located at 2θ = 15.19°, 17, 23°, 18.13°, 20.10° and 23.10°. According to Ramirez *et al*., with the addition of glycerin, the starch grains were restructured, causing modifications to the crystallographic profile [20]. In other words, the crystallinity of starch was significantly reduced, and tended to exist in highly amorphous conditions. Similar results were also reported in literature [20–26]. The other XRD patterns refer to the starch–NaOH complex films. No major alterations were spotted with the addition of NaOH up to 20 wt.%, and the diffractograms definitely have a similarity and exist in an amorphous state. Several peaks at 17.8°, 28.6°, 33.5°, 39.8° and 44.3° were clearly visible after the addition of 25-30wt.% of NaOH. The peaks at 17.8°, 39.8° and 44.3° corresponded to NaOH peaks, and the rests were probably matched with Na_2O and Na_2O_2[27]. From the XRD analyses, two conclusions can be made; first, the complex films were present in amorphous rather than crystalline condition, and NaOH did not wholly influence the crystallographic profile due to the incredibly amorphous nature of polymer and its incomplete crystalline structure, and second, the presence of a variation of peaks of the studied materials on the

crystallographic patterns had confirmed that the polymerization process had taken place in the solid polymer electrolyte preparation [28–30].

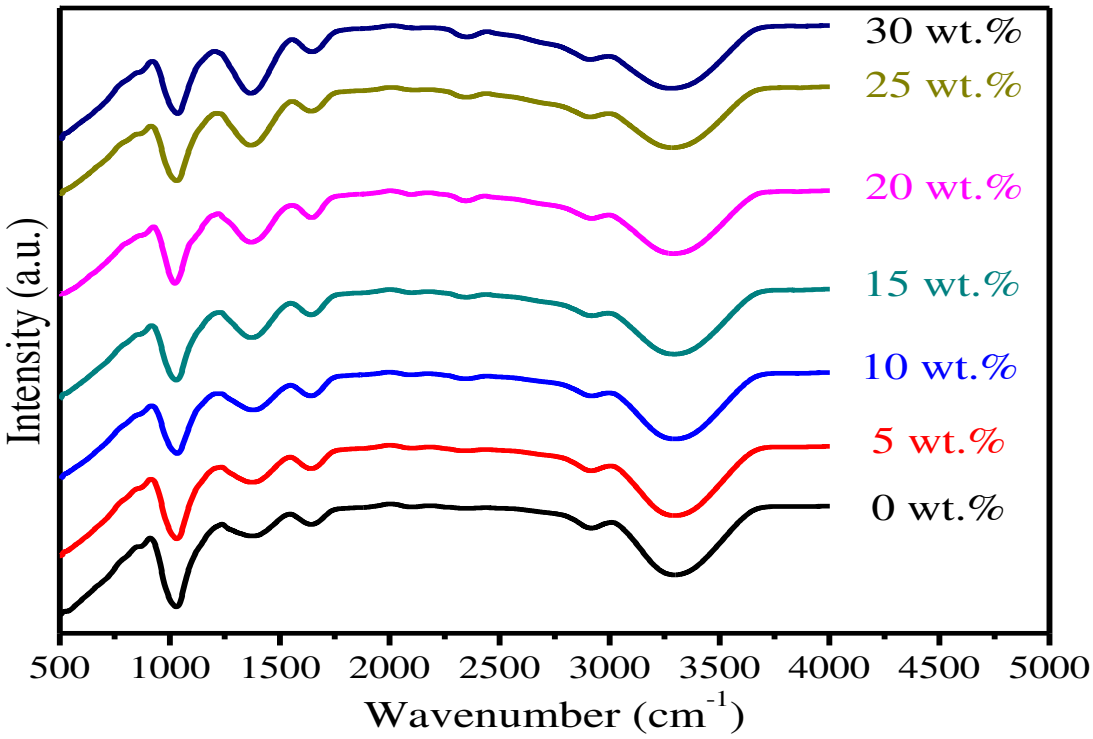

Figure-3. This FTIR patterns for starch and hybrid starch-NaOH films.

The FTIR spectra for the starch and starch–sodium hydroxide complex films are illustrated in Figure-3. In the figure, the IR spectrum of films shows characteristic absorption bands at 1036 cm^{-1}, 1382 cm^{-1}, 1643 cm^{-1}, 2916 cm^{-1} and 3304 cm^{-1}, respectively. The IR spectrum of films showed a CO stretching in the plane at 1036 cm^{-1} and an –OH bending vibration band at 1382 cm^{-1}. The FTIR spectrum of the as-prepared films also showed the band at 1643 cm^{-1} which was attributed to water adsorbed in the amorphous state and has been described to diverge based on crystallinity. The other peak located at 2916 cm^{-1} corresponds to the methyl group (-CH_2 stretching vibration). The prepared film also showed an –OH stretching peak at 3304 cm^{-1} due to water absorption. As can be seen in the complexed spectra, there are significant changes for all films, particularly in terms of their intensity. Specifically, the peak intensity increased as the amount of NaOH increased (1382 cm^{-1}) and decreased with respect to the addition of NaOH (2916 cm^{-1} and 3304 cm^{-1}, respectively). All of the corresponding bands have been summarized in Table-2. It was undoubtedly confirmed that significant modifications had taken place in the chemical structure due to the doping of NaOH into the starch chains. These results verified that NaOH has been embedded into starch in the polymerization process.

Table-2. FTIR absorbance, functional groups and references of starch–NaOH complex films.

V(cm^{-1}) related to the crystal system	Absorbance change	Functional group	Reference
1036	–	(CO stretching)	[31]
1382	Δ	(–OH bending vibration)	[32]
1643	–	Hydroxyl (–OH bending)	[33]
2916	∇	Methyl (–CH_2 stretching vibration)	[33]
3304	∇	Hydroxyl (–OH stretching)	[34]

**indicator: - not change; Δ increase; ∇ decrease

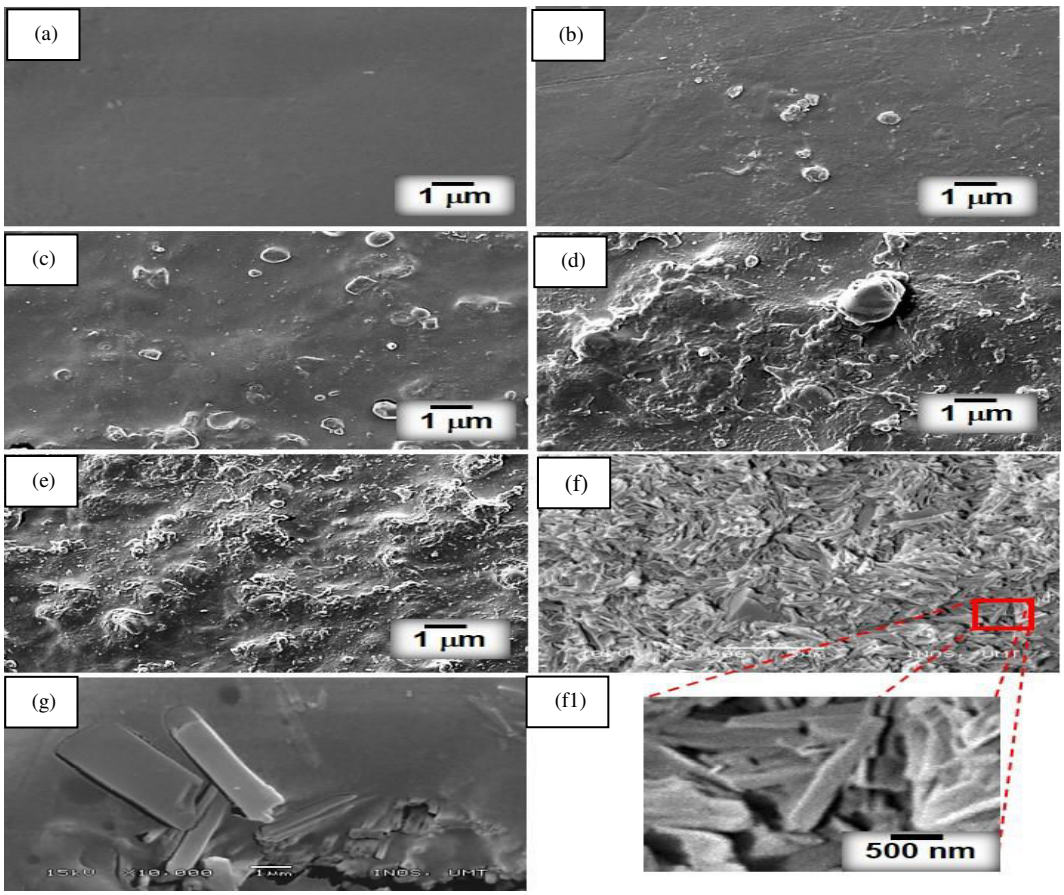

Figure-4. SEM micrographs for (a,) starch film, (b) 5 wt.% of NaOH (sample A), (c) 10 wt.% of NaOH (sample B), (d) 15 wt.% of NaOH (sample C), (e) 20 wt.% of NaOH (sample D), (f) 25 wt.% of NaOH (sample E) and (g) 30 wt.% of NaOH (sample F).

The morphologies of starch and hybrid starch–NaOH films are illustrated in Figure-4. A without dopant film had a smooth surface morphology (Figure-4a). The morphology had been altered with the presence of small quantities of round shapes on certain areas of the film after the addition of 5wt.% of NaOH. With the addition of 10wt.% of NaOH, the film did not change too much, but the round shape morphology had tripled in quantity compared to the previous film. The surface contour of the following samples (15, 20 and 25wt.%NaOH) was extremely modified with the presence of very tiny particles on top of the film surface (25wt.% NaOH). Remarkably, the tiny particles observed at high magnification were attributed to the belt shape morphology probably because the belt shape can be consistently found in the whole area of film. The belt shape structure had the width and length of around of 250 nm and 1.50 µm (Figure-4f1), respectively. With further additions of NaOH (25wt.%), the contour had changed to accommodate a bigger belt size (width = 1 µm and length = 2.5 µm) as shown in Figure 4g.

Table-3. The bulk resistance and ionic conductivity of starch–NaOH complex films.

Sample	Bulk resistance, R_b (Ω)	Conductivity, σ (S cm^{-1})
Pure	8.21×10^{3}	1.20×10^{-6}
A	1.18×10^{2}	1.14×10^{-4}
B	4.80×10^{1}	2.09×10^{-4}
C	1.50×10^{1}	7.36×10^{-4}
D	6.00×10^{0}	1.93×10^{-3}
E	2.70×10^{0}	3.93×10^{-3}
F	3.00×10^{1}	5.24×10^{-4}

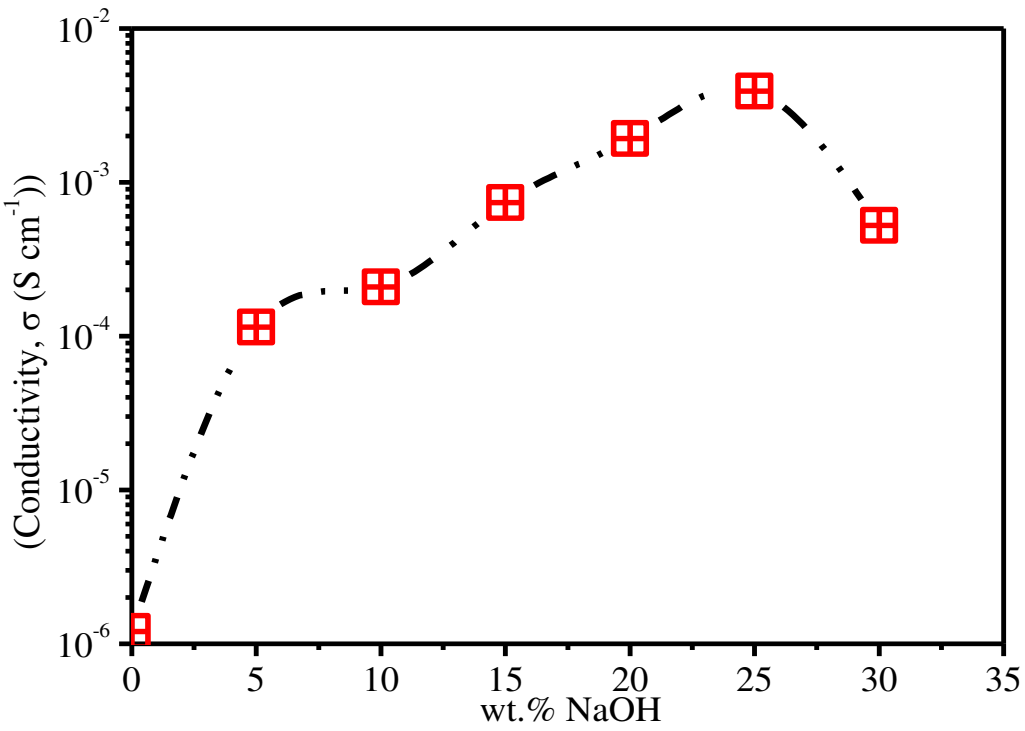

Figure-5. The conductivity variation as a function of salt content at room temperature.

The values of bulk resistance and conductivity are listed in Table-3, whereas the trend of conductivity versus salt content of prepared films is depicted in Figure-5. The measured thicknesses of the films were in between 0.009 to 0.049 cm. The bulk resistance of starch was 8.21 x 10^3 Ω with an ionic conductivity of approximately 1.20 x 10^{-6} S cm^{-1}. With the addition of 5 wt.% of NaOH to the polymer, the bulk resistance decreased to 1.18 x 10^2 Ω and the ionic conductivity increased to 1.14 x 10^{-4} S cm^{-1}. The bulk resistance (4.80 x 10^1 Ω) decreased after that, given the ionic conductivity of 2.09 x 10^{-4} S cm^{-1} for the film containing 10 wt.% of NaOH. With the addition of 15 wt.% of NaOH, the bulk resistance increased to 2.30 x 10^2 Ω and the ionic conductivity achieved was 4.80 x 10^{-5} S cm^{-1}). The measured resistance decreased to 5.10 x 10^1 Ω, while the ionic conductivity increased to 2.27 x 10^{-4} S cm^{-1} for the film with 20 wt.% of NaOH. The increasing trend of ionic conductivity continued for the film containing 25 wt.% of NaOH and its value was 1.07 x 10^{-3} S cm^{-1} with a bulk resistance of 2.7 Ω. With the addition of 30 wt.% of NaOH, the bulk resistance was increased; as a result, the ionic conductivity of film decreased (5.24 x 10^{-4} S cm^{-1}). With further additions of NaOH, the solution experienced low rigidity, thus causing the film to be hard to form. It was anticipated that the variation in ionic conductivity was attributed to the mobile–free ion associations occurring at low and high salt concentrations. At the medium salt concentrations, the dissociation and redissociation of salt had taken place [35, 36]. The drop in conductivity could be because of the increase in crystallinity as confirmed by the increase in intensity and the few peaks which emerged on the X–ray diffractogram. Besides that, another factor which contributed to the high ionic conductivity was the modification on the of film morphology to a belt–shape structure. According to literature, materials with belt–shape structures are well–known to have special properties such as effective improvisation of electrical conductivity, good mechanical strength, high catalytic activity and good electrochemical stability. We believed that this second factor might be the alternative side that contributed to the high ionic conductivity in the studied film [37, 38].

For comparison purposes, the method of synthesis, morphology and conductivity values of our prepared starch-NaOH microbelt films in this work and those of starch–based materials reported in the literature are summarized in Table 4. The results presented here show that the prepared starch–NaOH microbelt films possesses a fascinating structure and exhibit high ionic conductivity which is rarely documented in previous reports.

Table-4. Comparison of the conductivity value of hybrid starch–NaOH film prepared in this work with those of starch produced with different shapes and by different methods, as reported in literature.

Sample	Solvent	Morphology	Conductivity (S/cm)	Reference
Corn starch-NaOH	distilled water + glycerol	belts shape	3.39×10^{-3}	This work
Potato Starch-$Mg(C_2H_3O_2)_2$	acetic acid + glycerol	-	2.44×10^{-8}	[39]
Corn Starch-$LiPF_6$	distilled water	-	1.47×10^{-4}	[40]
Starch-KI	distilled water	-	7.02×10^{-3}	[41]
Potato Starch/Chitosan-$LiCF_3SO_3$	distilled water + ethanoic acid	-	7.11×10^{-7}	[42]
Potato starch-Sodium Salts	distilled water + glutaraldehyde + polyethylene glycol 300	-	1.12×10^{-4}	[43]
Rice Starch-LiI	distilled water	-	4.68×10^{-5}	[44]
Sago starch-KI	distilled water	entangled matrix	2.91×10^{-4}	[45]
Cassava Starch	glycerol	-	4.90×10^{-5}	[46]
Cassava Starch-Glycerol-Glutaraldehyde-Polyethyleneglycol-Lithium Perchlorate	water	granules	1.6×10^{-6}–8.1×10^{-3}	[47]
Corn starch-$LiClO_4$-$BaTiO_3$	water	aggregate and tail like chain particles	1.28×10^{-2}	[48]
Starch/Chitosan-NH_4NO_3	distilled water	-	3.89×10^{-5}	[49]
Corn starch–chitosan-NH_4I	acetic acid + deacetylation	granules	3.04×10^{-4}	[50]

CONCLUSIONS

In summary, a highly ionic conducting starch–NaOH polymer electrolyte film was prepared via a solution–casting technique. Interestingly, this simple preparation method had an important effect on the formation of a uniform dimension and a highly amorphous belt structure. The 25 wt.% starch–NaOH micro–belt film exhibited the highest ionic conductivity at as high as 3.39×10^{-3} S cm^{-1}. Two main factors were thought to contribute to the high conductivity values. First is the amorphous structure (belts-shape structure) of the complex film which acts as a supportive medium for fast ionic movement. The second factor is related to the inorganic salt which supplied free mobile ionic conductors to the closed system until a saturated condition was achieved. Combined with its unique characteristics of mentioned above, it is therefore expected that the present reported starch–NaOH micro–belt polymer electrolyte film can be a promising candidate material for application in energy storage devices.

ACKNOWLEDGEMENTS

The financial and facilities supports from School of Fundamental Science and School of Ocean Engineering are greatly appreciated.

REFERENCES

[1] Sing K., Tiwari R. U. and Deshpande V. K. 1993. Performance of a solid-state battery with a proton-conducting electrolyte.J. Power Source. 46, 65-71.

[2] Hiralal P., Imaizumi S., Unalan H. E., Matsumoto H., Minagawa M., Rouvala M., Tanioka A., Amaratunga A. J. 2010. Nanomaterial-Enhanced All-Solid Flexible Zinc-Carbon Batteries. ACS Nano. 5, 2730-2734.

[3] Fu J., Zhang J., Song X., Zarrin H., Tian X., Qiao J., Rasen L., Li K. and Chen Z. 2016. A flexible solid-state electrolyte for wide-scale integration of rechargeable zinc-air batteries. Energ. Environ. Sci. 9: 663-670.

[4] Zhang G. Q. and Zhang X. G. 2003. A novel alkaline Zn/MnO2 cell with alkaline solid polymer electrolyte. Solid State Ionics. 160: 155-159.

[5] Kotobukia M., Lua L., Savilovc S. V. and Aldoshin S. M. 2017. Poly(vinylidene fluoride)-Based Al Ion Conductive Solid Polymer Electrolyte for Al Battery. J. Electrochem. Soc. 164: A3868-A3875.

[6] Zhang Z., Zuo C., Liu Z., Yu Y., Zuo Y., Song Y. 2014. All-solid-state Al-air batteries with polymer alkaline gel electrolyte. J. Power Sources. 251: 470-475.

[7] Suren S. and Kheawhom S. 2016. Development of a High Energy Density Flexible Zinc-Air Battery. J. Electrochem. Soc. 163: A846-A850.

[8] Choi B. G., Hong J., Hong W. H., Hammond P. T. and Park H. 2011. Facilitated Ion Transport in All-Solid-State Flexible Super capacitors. ACS Nano. 5: 7205-7213.

[9] Lin Y., Li J., Liu K., Liu Y., Liu J. and Wang X. 2016. Unique starch polymer electrolyte for high capacity all-solid-state lithium sulfur battery. Green Chem. 18: 3796-3803.

[10] Okuo J., Emina A., Omorogbe S. and Anegbe B. 2018.Synthesis, characterization and application of starch stabilized zerovalent iron nanoparticles in the remediation of Pb-acid battery soil. Environ. Nanotechnol. Monit. Manage. 9: 12-17.

[11] Li W., Chen M. and Wang C. 2011. Spherical hard carbon prepared from potato starch using as anode material for Li-ion batteries. Mater. Lett. 65: 3368-3370.

[12] Kim Y., Kim J., Vaalma C., Bae G. H., Kim G., Passerini S. and Kim Y. 2018. Optimized hard carbon derived from starch for rechargeable seawater batteries. Carbon. 129: 564-571.

[13] Cheng K., Zhang F., Sun F., Chen H. and Zhang Y. P. 2015. Doubling Power Output of Starch Biobattery Treated by the Most Thermostable Isoamylase from an Archaeon Sulfolobustokodaii. Sci. Rep-UK. 5: 13184.

[14] Minakashi M. 2012. Looking beyond lithium-ion technology – Aqueous NaOH battery. Mater. Sci. Eng. B. 177: 1788-1792.

[15] Liu S., Pan G. L., Li G. R. and Gao X. P. 2015. Copper hexacyanoferrate nanoparticles as cathode material for aqueous Al-ion batteries. J. Mater. Chem. A. 3: 21039-21043.

[16] Mori R. 2015. Addition of Ceramic Barriers to Aluminum–Air Batteries to Suppress By-product Formation on Electrodes. J. Electrochem. Soc. 162: A288-A294.

[17] Erfani A., Muhammadi M., Neshat S. A., Shalchi M. M. and Varaminian F. 2015. Investigation of Aluminum Primary Batteries Based on Taguchi Method. Ener. Technol. Pol. 2: 19-27.

[18] Hassan M. F. and Noruddin N. 2018. The effect of lithium perchlorate on poly (sodium 4-styrenesulfonate): studies based on morphology, structural and electrical conductivity. Mater. Phys. Mech. 36: 8-17.

[19] Hassan M. F., Zainuddin S. K., Kamarudin K. H., Sheng C. K., Abdullah M. A. A. 2018. Ion-conducting polymer electrolyte films based on poly (sodium 4-styrenesulfonate) complexed with ammonium nitrate: studies based on morphology, structural and electrical spectroscopy. MJAS. 22: 238-248.

[20] Hizukuri S. 1961. X-Ray Diffractometric Studies on Starches. Agr. Biol. Chem. Tokyo. 25: 45-49.

[21] Srichuwong S., Isono N., Mishima T., Hisamatsu M. 2005. Structure of lintnerized starch is related to X-ray diffraction pattern and susceptibility to acid and enzyme hydrolysis of starch granules. Int. J. Biol. Macromol. 37: 115-121.

[22] Utrilla-Coello R. G., Hernandez-Jaimesa C., Carrillo-Navasa H., Gonzaleza F., Rodrigueza E., Bello-Perez L. A., Vernon-Cartera E. J. and Alvarez-Ramirez J. 2014. Acid hydrolysis of native corn starch: Morphology, crystallinity, rheological and thermal properties. Carbohyd. Polym. 103: 596-602.

[23] Han F., Gao C. and Liu M. 2013. Fabrication and Characterization of Size-Controlled Starch-Based Nanoparticles as Hydrophobic Drug Carriers. J. Nanosci. Nanotechno. 13: 6996-7007.

[24] Ramirez M. G. L., de. Muniz G. I. B., Satyanarayana K. G., Tanobe V., Iwakiri S. 2010. Preparation and characterization of biodegradable composites based on brazilian cassava starch, corn starch and green coconut fibers. Rev. Materia, 15: 330-337.

[25] Ma Z. And Boye J. I. 2016. Research advances on structural characterization of resistant starch and its structure-physiological function relationship. Crit. Rev. Food Sci. Nutr. 56: 1059-1083.

[26] Lian X., Cheng K., Wang D., Zhu W. and Wang X. 2017. Analysis of crystals of retrograded starch with sharp X-ray diffraction peaks made by

recrystallization of amylose and amylopectin. Int. J. Food Prop. 20: S3224-3236.

[27] Mao J., Gu Q. and Gregory D. H. 2015. Revisiting the Hydrogen Storage Behavior of the Na-O-H System. Materials. 8: 2191-2203.

[28] Ramesh S. and Liew C. 2012. Development and investigation on PMMA–PVC blend-based solid polymer electrolytes with LiTFSI as dopant salt. Polym. Bull. 70: 1277-1288.

[29] Patla S. K., Ray R., Asokan K. and Karmakar S. 2018. Investigation of ionic conduction in PEO–PVDF based blend polymer electrolytes. J. Appl. Phys. 123: 125102.

[30] Sheha E. M., Nasr M. M. and El-Mansy M. K. 2015. The role of $MgBr_2$ to enhance the ionic conductivity of PVA/PEDOT: PSS polymer composite. J. Adv. Res. 6: 563-569.

[31] He Y., Wu Z., Ye B., Wang J., Guan X. and Zhang J. 2016. Viability evaluation of alginate-encapsulated Pseudomonas putida Rs-198 under simulated salt-stress conditions and its effect on cotton growth. Eur. J. Soil Biol. 75: 135-141.

[32] Tongdeesoontorn W., Mauer L. J., Wongruong S., Sriburi P. and Rachtanapun P. 2011. Effect of carboxymethyl cellulose concentration on physical properties of biodegradable cassava starch-based films. Chem. Cent. J. 5: PMC3041729.

[33] Mukurumbira A., Mariano M., Dufresne A., Mellem J. J. and Amonsou E. O. 2017. Microstructure, thermal properties and crystallinity of amadumbe starch nanocrystals. Int. J. Biol. Macromol. 102: 241-247.

[34] Rachtanapun P., Simasatitkul P., Chaiwan W. and Watthanaworasakun Y. 2012. Effect of sodium hydroxide concentration on properties of carboxymethyl rice starch. IFRJ. 19: 923-931.

[35] Aziz S. B. 2018. The mixed contribution of ionic and electronic carriers to conductivity in chitosan based solid electrolytes mediated by cunt salt. J. Inorg. Organomet Polym. Mater. 1-11

[36] Gonzalez F., Gregorio V., Rubio A., Garrido L., GarciaN. and Tiemblo P. 2018. Ionic Liquid-Based Thermoplastic Solid Electrolytes Processed by Solvent-Free Procedures. Polymer. 10: 124.

[37] Guo Z., Wang F., Xia Y., Li J., Tamirat A. G., Liu Y., Wang L., Wang Y. and Xia Y. 2018. In situ encapsulation of core-shell-structured Co@Co3O4 into nitrogen-doped carbon polyhedra as a bifunctional catalyst for rechargeable Zn–air batteries. J. Mater. Chem. A. 6: 1443-1453.

[38] Padmanaban S., Kim M. and Yoon S. 2017. Size-tunable Synthesis of Silver Nanobelts Using a Polyaniline Derived Polymer as a Template. Sci. Rep.-UK. 7: 44796.

[39] Shukur M. F., Ithnin R. and Kadir M. F. Z. 2016. Ionic conductivity and dielectric properties of potato starch-magnesium acetate biopolymer electrolytes: the effect of glycerol and 1-butyl-3-methylimidazolium chloride. Ionics. 22: 1113-1123.

[40] Liew C. and Ramesh S. 2015. Electrical, structural, thermal and electrochemical properties of corn starch-based biopolymer electrolytes. Carbohyd. Polym. 124: 222-228.

[41] Bementaa E. And Rajan M. A. J. 2016. Electrical Dimensions and Enhancement of Ionic Conductivity of Mixing of KI in Biopolymeric Starch by Gelation Method. Mater. Today-Proc. 3: 3814-3819.

[42] Navaratnama S., Sanusia A., Ahmad A. H., Ramesh S., Ramesh K. and OthmanN. 2015. Conductivity studies of biopolymer electrolyte based on potato starch/chitosan blend doped with $LICF_3SO_3$. Journal Teknologi (Sci. Eng.) 75: 1-5.

[43] Tiwari T., Srivastava N. and Srivastava P. C. 2013. Ion Dynamics Study of Potato Starch + Sodium Salts Electrolyte System. Int. J. Electrochem. 2013: 670914.

[44] Khanmirzaei M. H. and Ramesh S. 2013. Ionic Transport and FTIR Properties of Lithium Iodide Doped Biodegradable Rice Starch Based Polymer Electrolytes. Int. J. Electrochem. Sci. 8: 9977-9991.

[45] Singh R., Singh P. K., Tomar S. K. and Bhattacharya B. 2016. Synthesis, characterization, and dye-sensitized solar cell fabrication using solid biopolymer electrolyte membranes. High Perform Polym. 28: 47-54.

[46] Ayala G., Agudelo A. and Vargas R. 2012. Effect of glycerol on the electrical properties and phase behavior of cassava starch biopolymers. Dyna. 171: 138-147.

[47] Arrieta A. A., Ganan P. F., Marqueza S. E. and Zuluaga R. 2011. Electrically Conductive Bioplastics from Cassava Starch. J. Braz. Chem. Soc. 22: 1170-1176.

[48] Teoh K. H., Lim C., Liew C. W. and Ramesh S. 2016. Preparation and performance analysis of barium titanate incorporated in corn starch-based polymer electrolytes for electric double layer capacitor application. J. Appl. Polym. Sci. 133: 43275.

[49] Khiar A. S. A. and Arof A. K. 2011. Electrical properties of starch/chitosan-NH_4NO_3 polymer electrolyte. Int. J. Physical Math. Sci. 5: 1662-1666.

[50] Yusof Y. M., Shukur M. F., Illias H. A., and Kadir M. F. Z. 2014. Conductivity and electrical properties of corn starch-chitosan blend biopolymer electrolyte incorporated with ammonium iodide. Phys. Scr. 89: 035701.